






# Structures and kinetics of *Thermotoga maritima* MetY reveal new insights into the predominant sulfurylation enzyme of bacterial methionine biosynthesis

Received for publication, December 24, 2020, and in revised form, May 12, 2021. Published, Papers in Press, May 18, 2021.

<https://doi.org/10.1016/j.jbc.2021.100797>

Jodi L. Brewster<sup>1</sup>, Petr Pachi<sup>2</sup>, James L. O. McKellar<sup>1</sup>, Maria Selmer<sup>3</sup> , Christopher J. Squire<sup>4</sup> , and Wayne M. Patrick<sup>5,\*</sup> 

From the <sup>1</sup>Department of Biochemistry, University of Otago, Dunedin, New Zealand; <sup>2</sup>Institute of Organic Chemistry and Biochemistry, Czech Academy of Sciences, Prague, Czech Republic; <sup>3</sup>Department of Cell and Molecular Biology, Uppsala University, Uppsala, Sweden; <sup>4</sup>School of Biological Sciences, University of Auckland, Auckland, New Zealand; <sup>5</sup>Centre for Biodiscovery, School of Biological Sciences, Victoria University of Wellington, Wellington, New Zealand

Edited by Ruma Banerjee

Bacterial methionine biosynthesis can take place by either the *trans*-sulfurylation route or direct sulfurylation. The enzymes responsible for *trans*-sulfurylation have been characterized extensively because they occur in model organisms such as *Escherichia coli*. However, direct sulfurylation is actually the predominant route for methionine biosynthesis across the phylogenetic tree. In this pathway, most bacteria use an *O*-acetylhomoserine aminocarboxypropyltransferase (MetY) to catalyze the formation of homocysteine from *O*-acetylhomoserine and bisulfide. Despite the widespread distribution of MetY, this pyridoxal 5'-phosphate-dependent enzyme remains comparatively understudied. To address this knowledge gap, we have characterized the MetY from *Thermotoga maritima* (*Tm*MetY). At its optimal temperature of 70 °C, *Tm*MetY has a turnover number (apparent  $k_{\text{cat}} = 900 \text{ s}^{-1}$ ) that is 10- to 700-fold higher than the three other MetY enzymes for which data are available. We also present crystal structures of *Tm*MetY in the internal aldimine form and, fortuitously, with a  $\beta,\gamma$ -unsaturated ketimine reaction intermediate. This intermediate is identical to that found in the catalytic cycle of cystathionine  $\gamma$ -synthase (MetB), which is a homologous enzyme from the *trans*-sulfurylation pathway. By comparing the *Tm*MetY and MetB structures, we have identified Arg270 as a critical determinant of specificity. It helps to wall off the active site of *Tm*MetY, disfavoring the binding of the first MetB substrate, *O*-succinylhomoserine. It also ensures a strict specificity for bisulfide as the second substrate of MetY by occluding the larger MetB substrate, cysteine. Overall, this work illuminates the subtle structural mechanisms by which homologous pyridoxal 5'-phosphate-dependent enzymes can effect different catalytic, and therefore metabolic, outcomes.

Methionine is essential for all organisms. As a proteinogenic amino acid, it has roles in translation initiation, protein folding, stability, and function (1). Methionine residues are also sites of post-translational modification, particularly by oxidation. Methionine is the precursor of *S*-adenosyl methionine, which is an important intracellular carrier of methyl groups. Thus, methionine occupies a central role in the metabolic network (2, 3).

The biosynthesis of methionine occurs in plants and microorganisms (3–5), but not in animals. The first bacterial biosynthetic pathways to be studied in detail were from the model  $\gamma$ -proteobacteria *Escherichia coli* and *Salmonella typhimurium* (6–8). In these species, two enzymes (encoded by *metB* and *metC*) are used to convert *L*-*O*-succinylhomoserine (*L*-OSHS) into the penultimate intermediate, homocysteine (Fig. 1). However, this *trans*-sulfurylation pathway is the exception, and not the rule, across the phylogenetic tree of bacteria (3). Outside of the  $\beta$ - and  $\gamma$ -proteobacteria, it is rare to use *L*-OSHS as the activated substrate for sulfurylation. It is far more common to use *L*-*O*-acetylhomoserine (*L*-OAHS) instead (9). The two-step *trans*-sulfurylation route is similarly uncommon outside of the  $\gamma$ -proteobacteria (3). Most bacteria carry out a one-step conversion of *L*-OAHS (or *L*-OSHS) to homocysteine or even directly to methionine (Fig. 1). This direct sulfurylation is catalyzed by acylhomoserine transferase enzymes that are the products of genes most commonly annotated as *metY* and sometimes as *metZ* (3). Confusingly, the equivalent gene is named *metC* in *Mycobacterium* species, including *Mycobacterium tuberculosis* (10, 11).

Confusion around the sulfurylation enzymes extends beyond gene names and into their biochemistry. The enzymes of the *trans*-sulfurylation and direct sulfurylation routes are all homologues, and they all use pyridoxal 5'-phosphate (PLP) as a cofactor. PLP-dependent enzymes catalyze a broad range of reactions in amino acid metabolism, but at the same time, they display low levels of sequence identity (12–16). These features make it difficult to ascribe functions accurately from sequence information alone. For example, the InterPro database (17) categorizes the *metY*-encoded enzymes (InterPro family

\* For correspondence: Wayne M. Patrick, [wayne.patrick@vuw.ac.nz](mailto:wayne.patrick@vuw.ac.nz).

Present address for Jodi L. Brewster: Molecular Horizons, School of Chemistry and Molecular Bioscience, University of Wollongong, NSW 2522, Australia.

## Structure and function of *Thermotoga maritima* MetY

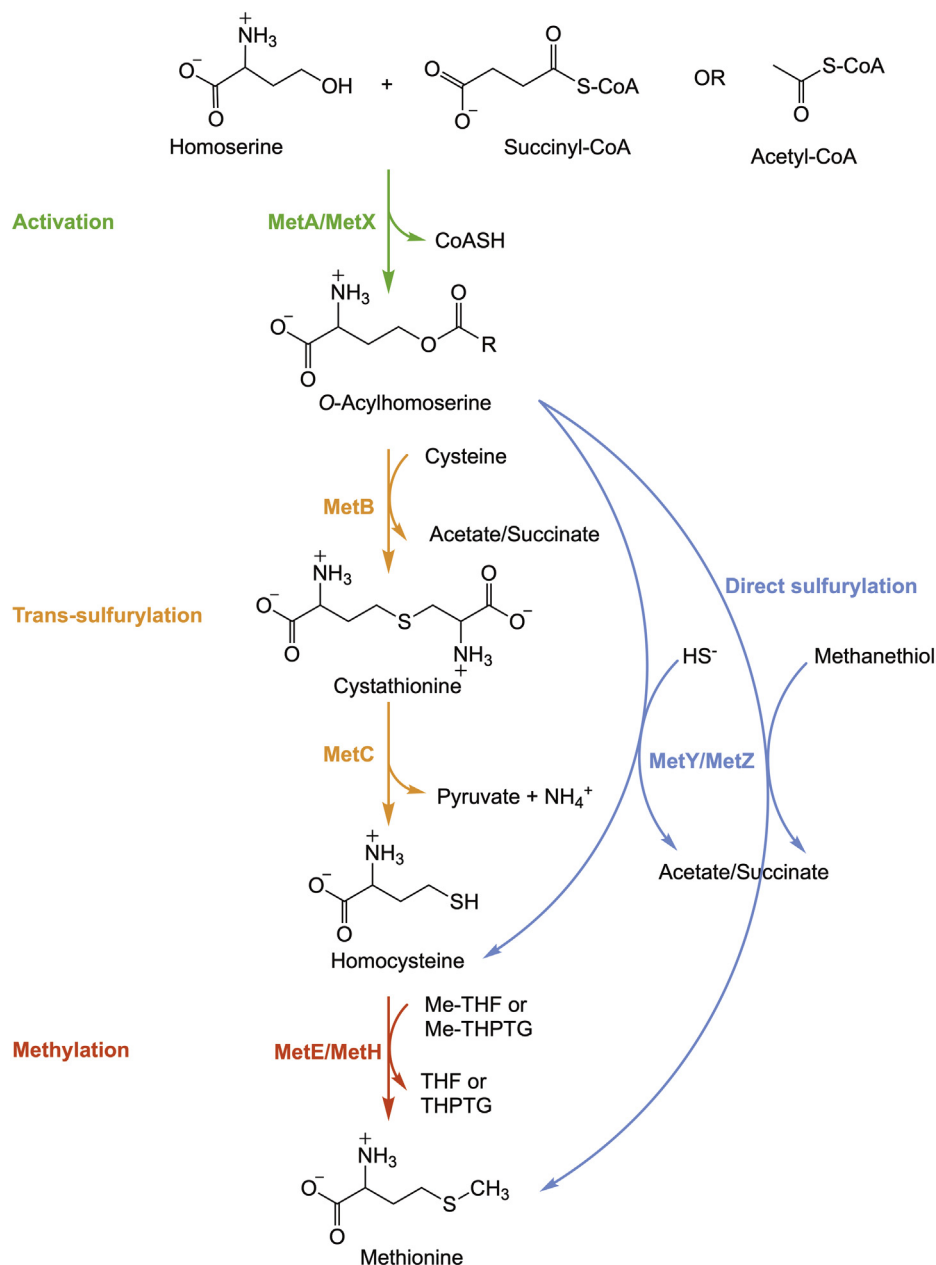


**Figure 1. Bacterial methionine biosynthesis pathways.** Me-THF, 5-methyl-tetrahydrofolate; Me-THPTG, 5-methyltetrahydropteroyl tri-L-glutamate; THF, tetrahydrofolate; THPTG, tetrahydropteroyl tri-L-glutamate.

IPR006235) as those that utilize L-OAHS and the *metZ*-encoded enzymes (InterPro family IPR006234) as those that utilize L-OSHS. However, almost all *metZ*-encoded enzymes occur in organisms that produce L-OAHS rather than the predicted substrate L-OSHS, and no *metZ*-encoded enzyme has actually had its substrate preference characterized biochemically (3).

When taxonomic diversity is considered, the prevalent route for sulfurylation in bacterial methionine biosynthesis is by using a *metY*-encoded enzyme and bisulfide ( $\text{HS}^-$ ) as the sulfur source (Fig. 1) (3). An enzyme with this activity is also likely to have been the common ancestor of all sulfurylation enzymes (18). The *metY*-encoded enzymes were

originally classified as lyases in Enzyme Commission (EC) class 4.2.99.10 and were variously known as *O*-acetylhomoserine sulfhydrylases, *O*-acetylhomoserine (thiol)-lyases or *O*-acetylhomoserine thiolases. However, they have subsequently been reclassified as transferases (EC 2.5.1.49) with the systematic name of *O*-acetylhomoserine amino-carboxypropyltransferases. For simplicity, we refer to a *metY*-encoded enzyme as MetY.

The absence of MetY from model organisms such as *E. coli* means it is a comparatively understudied link in the bacterial methionine biosynthesis pathway. With respect to steady-state kinetics, the BRENDA database (19) currently contains Michaelis–Menten constants (*i.e.*,  $K_M$  values) for

only four bacterial enzymes. To the best of our knowledge, the *Corynebacterium glutamicum*, *Clostridioides difficile*, and *Clostridium novyi* MetY enzymes are the only three for which a turnover number ( $k_{\text{cat}}$ ) and therefore a catalytic efficiency ( $k_{\text{cat}}/K_M$ ) have been reported (20–22), although the *C. glutamicum* enzyme is bifunctional and acts almost as efficiently as a cystathionine  $\gamma$ -synthase (MetB) (20). Only one MetY structure, from *Wolinella succinogenes*, has been described in the literature (23). However, this enzyme is unusual because the sulfur donor is not bisulfide but instead a sulfur-carrier protein in which the C-terminal carboxylate has been modified to a thiocarboxylate. Atomic coordinates have also been deposited in the Protein Data Bank (PDB) for the functionally validated MetY from *Thermus thermophilus* (24, 25) and a third enzyme, from *Campylobacter jejuni* (26), although its function as an MetY has not yet been confirmed biochemically.

Although there is a paucity of data on MetY, MetB (EC 2.5.1.48) is a paradigm for understanding specificity, mechanism, and structure–function relationships in the *trans*-sulfurylation enzymes and their homologues from cysteine metabolism (27, 28). MetB catalyzes a highly similar  $\gamma$ -replacement reaction to MetY, using L-cysteine as a second substrate instead of HS<sup>−</sup> to yield cystathionine instead of homocysteine (Fig. 1). The reaction mechanism of the L-OSHS-dependent *E. coli* MetB (*EcMetB*) has been investigated extensively (28–30). Its structure has also been solved (31), and it is a well-studied exemplar of the fold type I PLP-dependent enzymes (14, 32). In addition to their shared mechanistic aspects, MetY and MetB are also close structural homologues (23).

In this work, we set out to investigate the determinants of specificity that distinguish MetY from MetB. In a previous study, we purified the *Thermotoga maritima* MetY (*TmMetY*; UniProt entry Q9WZY4) and showed by nonquantitative MS that it catalyzed the formation of homocysteine from L-OAHS and HS<sup>−</sup> (33). Here, we present an in-depth functional and structural study of the enzyme. We are the first to report both steady-state kinetics and structures for a MetY enzyme and also the first to describe the structure of an O-acylhomoserine-utilizing MetY. Of particular note, one of our two X-ray crystal structures fortuitously captured a reaction intermediate, shedding light on the mechanism and determinants of specificity in this widespread enzyme from a central metabolic pathway.

## Results and discussion

### Assay design and implementation

To measure *TmMetY* activity, we required a robust assay for quantifying L-homocysteine. A common method for the detection of thiolated reaction products is by the reduction of Ellman's reagent [5,5'-dithiobis (2-nitrobenzoic acid)], which can be quantified spectrophotometrically (34). However, one of the substrates in the reaction catalyzed by *TmMetY* is free thiol, which instantaneously saturates the colorimetric reaction and renders this method ineffective. In clinical settings,

homocysteine is commonly quantified by reversed-phase HPLC. However, this method requires the additional preparation steps of thiol reduction and derivatization for absorbance- or fluorescence-based detection (35, 36). These processes present challenges for generating Michaelis–Menten kinetics parameters, such as the optimization of reduction and derivatization reactions, the potential for product loss therein, the interpretation of complex elution profiles, and poor reproducibility (37).

These concerns prompted us to search for a homocysteine quantitation method that was better suited to analyzing enzyme kinetics. We discovered a commercial product (from Diazyme Laboratories) marketed for the determination of homocysteine concentration in human blood plasma. This kit-based reaction couples the production of homocysteine in a primary end-point reaction to the oxidation of NADH in a series of secondary reactions (Fig. S1A). This series of reactions could be monitored spectrophotometrically by a decrease in absorbance at 340 nm. Critically for this study, the first stage of this discontinuous assay (*i.e.*, the *TmMetY*-catalyzed formation of L-homocysteine) could be performed at physiologically relevant temperatures of up to 80 °C. The second reaction for the detection of L-homocysteine was then performed at 37 °C and the amount quantified by reference to a standard curve (Fig. S1B).

### Determination of optimal reaction conditions

With our new quantitative assay in hand, we set out to determine the pH and temperature optima for the reaction catalyzed by *TmMetY*. Specific activities were compared across the range of pH 5.5 to 9.0. This required the use of two different buffers to ensure buffering capacity was maintained across the pH range: MES for pH 5.5 to 7.0 and bicine for pH 7.5 to 9.0. The optimal pH was found to be 7.0 (Fig. 2A). We then checked that the activity profile was not a reflection of buffer preference by comparing enzyme activity at pH 7.0 in several different buffers including MES, bicine, Tris HCl, potassium phosphate, MOPS, and HEPES. The specific activity was marginally higher in both bicine and HEPES, so the latter was chosen for all subsequent assays as the optimal *TmMetY* pH of 7.0 coincides with its effective buffering range (pH 6.8–8.2, compared with pH 7.6–9.0 for bicine) (38). Of note, the optimal pH also corresponds to the  $pK_a$  for dissociation of H<sub>2</sub>S into HS<sup>−</sup>.

Next, we determined the optimal temperature ( $T_{\text{opt}}$ ) for activity of the enzyme. *T. maritima* grows at temperatures between 55 °C and 90 °C (39), and in culture, the  $T_{\text{opt}}$  for growth is 80 °C (39, 40). Therefore, we expected the  $T_{\text{opt}}$  of *TmMetY* would coincide with this range. Enzyme activity in our *in vitro* assay was found to peak at 70 °C (Fig. 2B), after which it decreased dramatically so that at 80 °C the activity was lower than at 37 °C. We observed a similar trend, and the same  $T_{\text{opt}}$  of 70 °C, in our previous characterization of the multifunctional *T. maritima* cystathionine  $\beta$ -lyase (33). We also monitored thermal denaturation of *TmMetY* using a fluorescence thermal shift assay. Protein unfolding occurred

## Structure and function of *Thermotoga maritima* MetY

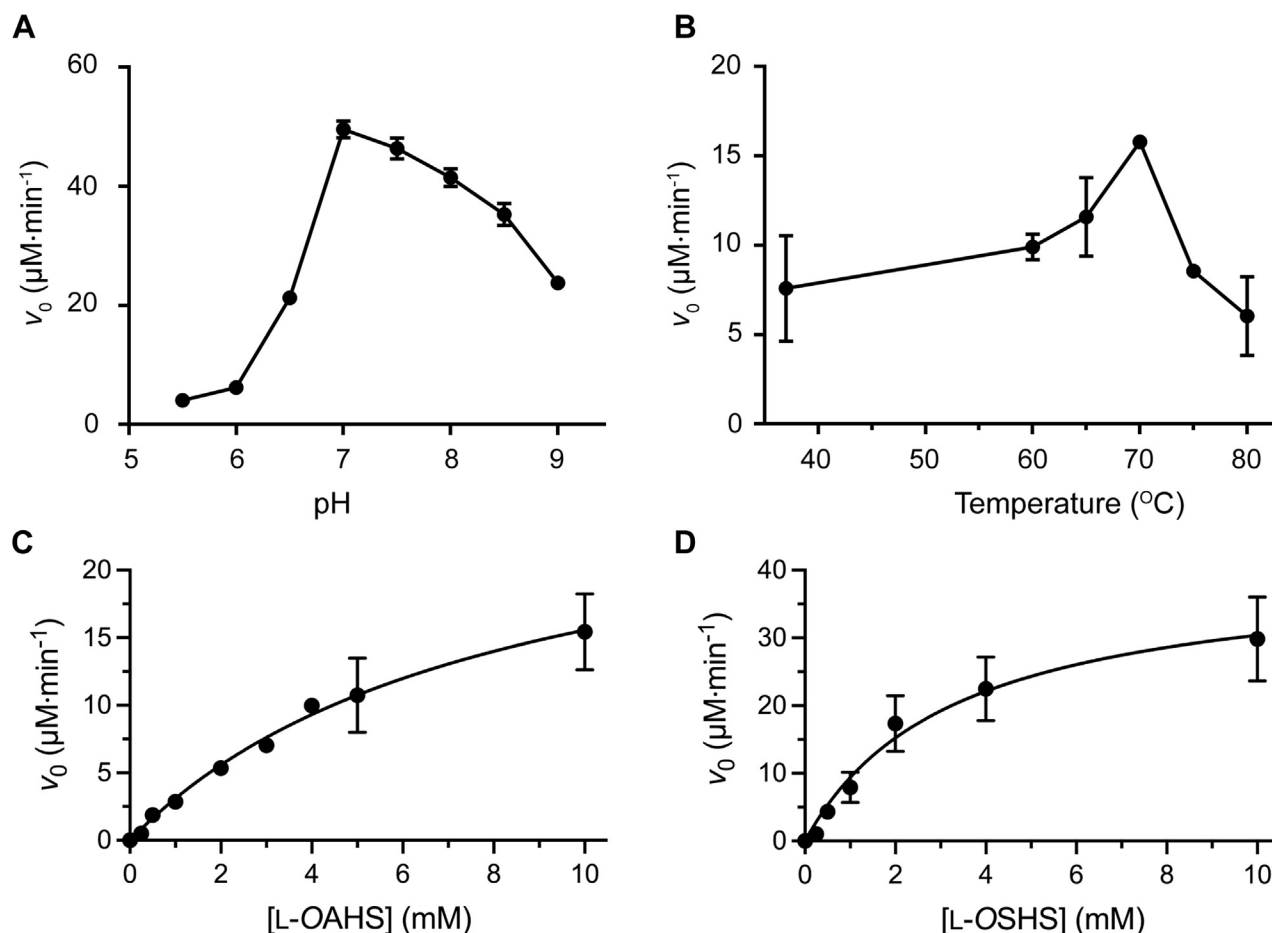


**Figure 2. Analyzing the catalytic activity of *TmMetY*.** *A*, the activity versus pH in assays conducted at 70 °C. *B*, the activity versus temperature in assays conducted at pH 7.0. In panels *A* and *B*, the reaction measured was the conversion of L-OAHS and HS<sup>-</sup> to homocysteine. *C* and *D*, fit of the Michaelis–Menten equation to the initial rate data when the substrate was L-OAHS (*C*) and when it was L-OSHS (*D*). Note that the concentration of the enzyme, *TmMetY*, was 0.5 nM for the assays in panel *C* but 2  $\mu\text{M}$  for the assays in panel *D*. Error bars indicate the standard error from two independently prepared batches of *TmMetY*, each assayed in technical duplicates. L-OAHS, L-O-acetylhomoserine; L-OSHS, L-O-succinylhomoserine; *TmMetY*, *Thermotoga maritima* MetY.

rapidly from 85 °C, with the melting temperature calculated to be 87 °C  $\pm$  1 deg. C.

### Steady-state kinetics with L-OAHS and L-OSHS

Having determined the optimal conditions for *TmMetY* activity *in vitro*, we next analyzed the steady-state kinetics of the reaction with respect to the native substrate L-OAHS. All previous studies on MetY enzymes (except for the bifunctional MetY/MetB from *C. glutamicum*) have found  $K_M$  values for the second substrate, bisulfide, to be in the range of 0.05 to 1.3 mM (21, 22, 41–44). Following the protocol established for assaying the thermostable MetY from *T. thermophilus* (43), we therefore fixed the bisulfide concentration at 5 mM.

The enzyme exhibited apparent Michaelis–Menten kinetics with L-OAHS, at 70 °C and pH 7.0 (Fig. 2C). The apparent  $k_{\text{cat}}$  ( $k_{\text{cat}}^{\text{APP}}$ ) with respect to this substrate was calculated to be 900 s<sup>-1</sup> per active site and the apparent  $K_M$  ( $K_M^{\text{APP}}$ ) for L-OAHS was 8 mM, giving a catalytic efficiency of  $k_{\text{cat}}^{\text{APP}}/K_M^{\text{APP}} = 1 \times 10^5$  s<sup>-1</sup> M<sup>-1</sup>. Given the complexity of the multistep assay and the corresponding noise in the standard curves we were able to generate (e.g., Fig. S1B), we have

deliberately reported these estimates at a level of precision that we believe to be justified. More precise determinations of the steady-state kinetic parameters are likely to require an alternate assay design. Despite these caveats, it is clear that the turnover number of *TmMetY* is significantly greater than the others that have been reported (Table 1). The apparent Michaelis constant for L-OAHS is similar to those reported for other bacterial and fungal MetY enzymes which, with the exception of the *C. novyi* and *C. difficile* MetY enzymes (Table 1), fall in the range of  $K_M = 1.9$  to 7.0 mM (20, 41–43, 45–47).

We previously showed that *TmMetY* could not accept L-cysteine in place of HS<sup>-</sup>; that is, it could not catalyze the formation of cystathionine (33). Here, we also tested whether *TmMetY* could accept L-OSHS instead of L-OAHS. This has been reported as a minor side activity of the MetY enzymes from *T. thermophilus* (relative activity of 1.4% compared with L-OAHS) and *Neurospora crassa* (relative activity of 0.15%) (41, 43). In contrast, enzymes from other bacterial species, including *C. novyi* and *C. difficile* (Table 1), lack activity with L-OSHS (21, 22, 42, 46). We were able to obtain Michaelis–

**Table 1**  
Steady-state kinetic parameters for selected MetY enzymes

Enzyme	Substrate	$k_{\text{cat}}$ ( $\text{s}^{-1}$ ) <sup>a</sup>	$K_M$ (mM) <sup>a</sup>	$k_{\text{cat}}/K_M$ ( $\text{s}^{-1} \text{M}^{-1}$ )	Reference
<i>T. maritima</i> MetY	L-OAHS	900 ± 200	8 ± 2	1 × 10 <sup>5</sup>	This work
	L-OSHS	0.3 ± 0.1	3 ± 1	1 × 10 <sup>2</sup>	This work
<i>C. novyi</i> MetY	L-OAHS	1.3	0.1	1.3 × 10 <sup>4</sup>	(22)
	L-OSHS	ND <sup>b</sup>	ND <sup>b</sup>	ND <sup>b</sup>	(22)
<i>C. difficile</i> MetY	L-OAHS	94	0.6	1.6 × 10 <sup>5</sup>	(21)
	L-OSHS	ND <sup>b</sup>	ND <sup>b</sup>	ND <sup>b</sup>	(21)
<i>C. glutamicum</i> MetY <sup>c</sup>	L-OAHS	28	6.4	4.4 × 10 <sup>3</sup>	(20)

<sup>a</sup> Standard errors are reported for two independently prepared batches of *Tm*MetY, each assayed in technical duplicate.

<sup>b</sup> ND, not detected.

<sup>c</sup> This enzyme also has a  $k_{\text{cat}}/K_M$  of 1.2 × 10<sup>3</sup> s<sup>-1</sup> M<sup>-1</sup> for the MetB reaction.

Menten kinetics with *Tm*MetY and L-OSHS (Fig. 2D), although the turnover number was reduced ~3000-fold relative to L-OAHS ( $k_{\text{cat}}^{\text{APP}} = 0.3 \text{ s}^{-1}$ ). A slightly lower  $K_M^{\text{APP}}$  resulted in an overall decrease of ~1000-fold in catalytic efficiency (Table 1). The enzyme preceding *Tm*MetY in *T. maritima* methionine biosynthesis, MetA, can catalyze the formation of L-OSHS from succinyl-CoA and homoserine, albeit 30-fold less effectively than its preferred reaction to form L-OAHS from acetyl-CoA and homoserine (48). It is therefore possible that some L-OSHS may be available in the metabolite pool under some circumstances and that *Tm*MetY may be able to salvage this otherwise dead-end metabolite.

### X-ray crystal structures of *Tm*MetY

We used X-ray crystallography to solve the structure of *Tm*MetY in its internal aldimine form and also in an intermediate-bound state, to resolutions of 2.00 Å and 2.22 Å, respectively (Table 2). Both structures show residues 2 to 429, and as reported previously for the *W. succinogenes* enzyme (23), they adopt an  $\alpha/\beta$ -fold containing 13  $\alpha$ -helices,

four  $3_{10}$ -helices (H7, H8, H9, and H15), and ten  $\beta$ -strands (Fig. S2). These elements are organized into three domains, which is characteristic of all fold type I PLP-dependent enzymes including the sulfurylation enzymes from methionine biosynthesis (14, 31, 32). Following the nomenclature established for MetB (31), the small N-terminal domain (residues 2–62) contributes to tetramer formation and consists of helices 1 and 2 interconnected by a long loop. The large PLP-binding domain (residues 63–288) is formed from a seven-stranded  $\beta$ -sheet (S1–S7) surrounded by helices (H3–H11) and contains the catalytic residues including the Schiff base-forming Lys210, which covalently links the PLP coenzyme. The longest  $\alpha$ -helix, H12, has one  $3_{10}$ -helical turn, resulting in a bend of approximately 65° that allows it to curve across the surface and bridge both the body and C-terminal domains. The C-terminal domain contains a four-stranded  $\beta$ -sheet (S8–S11) that forms the substrate binding pocket area of the active site and is encapsulated by helices H13–H17.

The MetY homologues MetB and cystathionine  $\beta$ -lyase are homotetramers in their active forms (31, 49–51), which is

**Table 2**  
X-ray crystallography data collection and refinement statistics

Data or statistic	7KB0 Internal aldimine	7KB1 Intermediate bound
Beamline	AS-MX2	AS-MX2
Wavelength (Å)	0.9537	0.9537
Resolution (Å) (outer shell)	42.88–1.85 (1.96–1.86)	48.37–1.85 (1.90–1.85)
Number of chains in the asymmetric unit	1	4
Space group	<i>P</i> 6 <sub>4</sub> 22	<i>P</i> 2 <sub>1</sub>
Cell dimensions		
<i>a</i> , <i>b</i> , <i>c</i> (Å)	135.24, 135.24, 110.85	67.58, 151.34, 91.39
$\alpha$ , $\beta$ , $\gamma$ (°)	90.0, 90.0, 120.0	90.0, 112.0, 90.0
$R_{\text{meas}}$ (outer shell)	0.25 (1.87)	0.05 (0.53)
$I/\sigma I$ (outer shell)	7.13 (1.16)	11.2 (1.87)
Completeness (%) (outer shell)	99.4 (99.6)	92.8 (72.7)
Multiplicity (outer shell)	7.6 (7.8)	2.5 (2.3)
Total no. of reflections (outer shell)	389,307 (63,168)	334,154 (17,815)
No. of unique reflections (outer shell)	51,081 (8154)	134,424 (7815)
Redundancy (outer shell)	7.6 (7.8)	2.4 (2.3)
Mean half-set correlation, $CC_{(1/2)}$ (outer shell)	0.99 (0.30)	0.99 (0.78)
Wilson B factor (Å <sup>2</sup> )	31.7	36.2
Refinement statistics		
No. of reflections (no. of test reflections)	51,080 (2590)	134,416 (6825)
$R_{\text{work}}/R_{\text{free}}$	0.21 (0.24)	0.23 (0.26)
No. of atoms: protein/ligands/water	3469/24/177	12,963/74/605
B factors: protein/ligands/water (Å <sup>2</sup> )	29.1/21.1/32.4	42.1/38.4/38.2
RMSD: bond lengths/bond angles (Å/°)	0.014/1.244	0.003/0.596
Ramachandran plot statistics		
Favored regions	96.7%	96.8%
Allowed regions	3.3%	3.2%
Outliers	0	0

## Structure and function of *Thermotoga maritima* MetY

consistent with our gel-permeation chromatography elution profile of *TmMetY* and also with data reported for *W. succinogenes* MetY (23). Our internal aldimine structure was solved with a single subunit in the asymmetric unit, and the tetramer (dimer of dimers) was generated by crystallographic symmetry. The intermediate-bound structure was solved with the complete tetramer in the asymmetric unit. The active site of *TmMetY* is located at the dimer interface, with four active sites per homotetramer, each involving residues from both chains in catalysis. In the internal aldimine form, PLP is covalently bound to Lys210 *via* a Schiff base linkage (Fig. 3).

Tetramers of the internal aldimine and intermediate-bound structures were close to identical, with an RMSD of 0.32 Å over all 1712 C $\alpha$  atoms (428 per subunit; Fig. S3A). In the intermediate-bound structure, the pyridine ring of PLP was rotated 11° upward (with N1 of PLP as the pivot point), toward Tyr113, relative to the internal aldimine (Fig. S3, B and C). Similar changes in the tilt of the pyridine ring of PLP have also been observed between internal and external aldimine forms of the *E. coli* cystathionine  $\beta$ -lyase (51, 52). In these cases, movements of the pyridine ring led to corresponding shifts in the position of the neighboring tyrosine side chain (equivalent to Tyr113 in *TmMetY*). In contrast, the position of Tyr113 in *TmMetY* is not perturbed by rotation of the coenzyme. Instead, Asn161 was the only side chain of the active site that moved (Fig. S3B). This appears to be due to the release of the covalently bound cofactor leading to a minor change in the position of its O3 hydroxyl group. The slight shift of the Asn161 carboxamide group shortens the hydrogen bond it forms with O3, from approximately 3.3 Å in the internal aldimine to 2.9 Å.

### *TmMetY* structure captures a reaction intermediate

The intermediate-bound structure (PDB ID: 7KB1) was obtained by soaking crystals with the favored substrate L-OAHS. However, during model building, it was obvious that we had not captured PLP–OAHS in the structure because the electron density extending from C4 of PLP was not large enough to accommodate it. After an initial refinement of the structure, bulk solvent-subtracted Polder OMIT maps (53) were constructed using phenix.polder (Fig. 4A and Fig. S4). Based on the OMIT maps, we constructed a model where, in chains A, B, and C, PLP was linked *via* a Schiff base to a derivative of L-OAHS (Fig. 4, B–D).

In chain D, it was clear that PLP was not in the internal aldimine state: the linkage between Lys210 and PLP was broken; the terminal amine of Lys210 was oriented away from the PLP aldehyde; and the pyridine ring of the cofactor had rotated toward its external aldimine position (Fig. 4E). However, the electron density was not sufficient to support the presence of the PLP-intermediate complex, so we have tentatively modeled free PLP into the active site. Complete X-ray photoreduction of the Schiff base has been observed in the crystallographic structure of a different PLP-dependent enzyme, alanine:glyoxylate aminotransferase (54). Although speculative, we propose radiation damage may also have been responsible for the unexpected cofactor density we observed in chain D of the intermediate-bound tetramer.

To our knowledge, a formal mechanism for MetY has not been proposed. However, MetB catalyzes an analogous  $\gamma$ -replacement in the *trans*-sulfurylation pathway (Fig. 1) and its mechanism is well-established (28–30). The key intermediate is a  $\beta,\gamma$ -unsaturated ketimine that is formed by elimination of succinate from L-OSHS. Our crystallographic data are

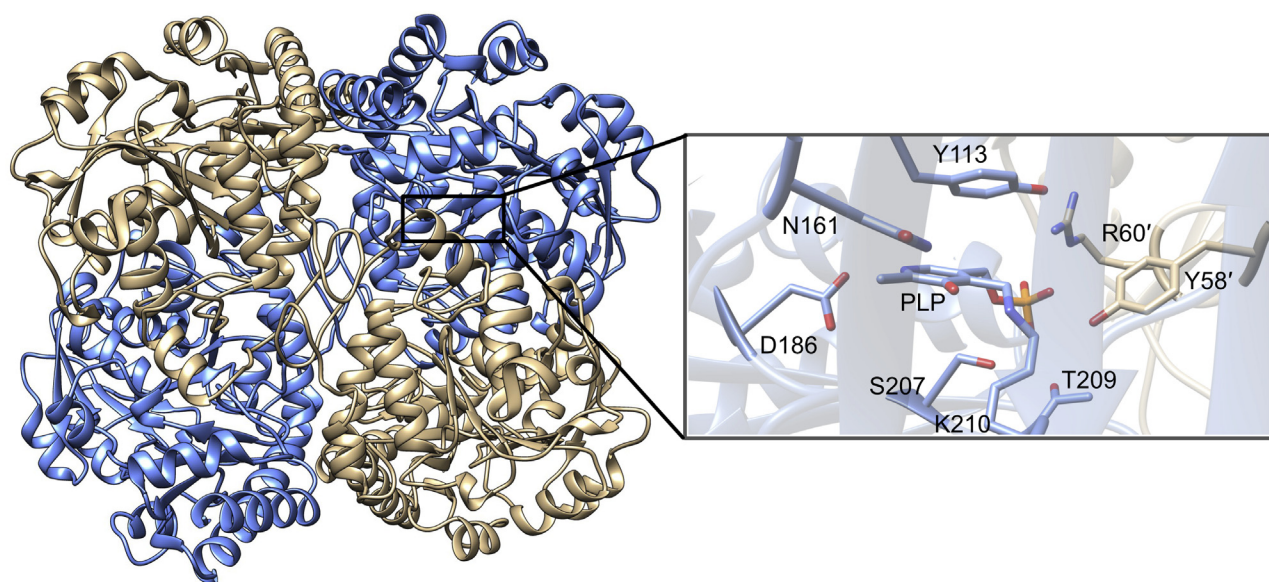


**Figure 3. X-ray crystallographic structure of *TmMetY*.** The native tetramer was reconstructed by applying symmetry operators to the asymmetric unit. A close-up of one of the four active sites in the tetramer is shown. The PLP coenzyme is in the internal aldimine configuration, bound to Lys210 through a Schiff base linkage. Residues labeled with a prime are from a different subunit than those that lack a prime. PLP, pyridoxal 5'-phosphate; *TmMetY*, *Thermotoga maritima* MetY.

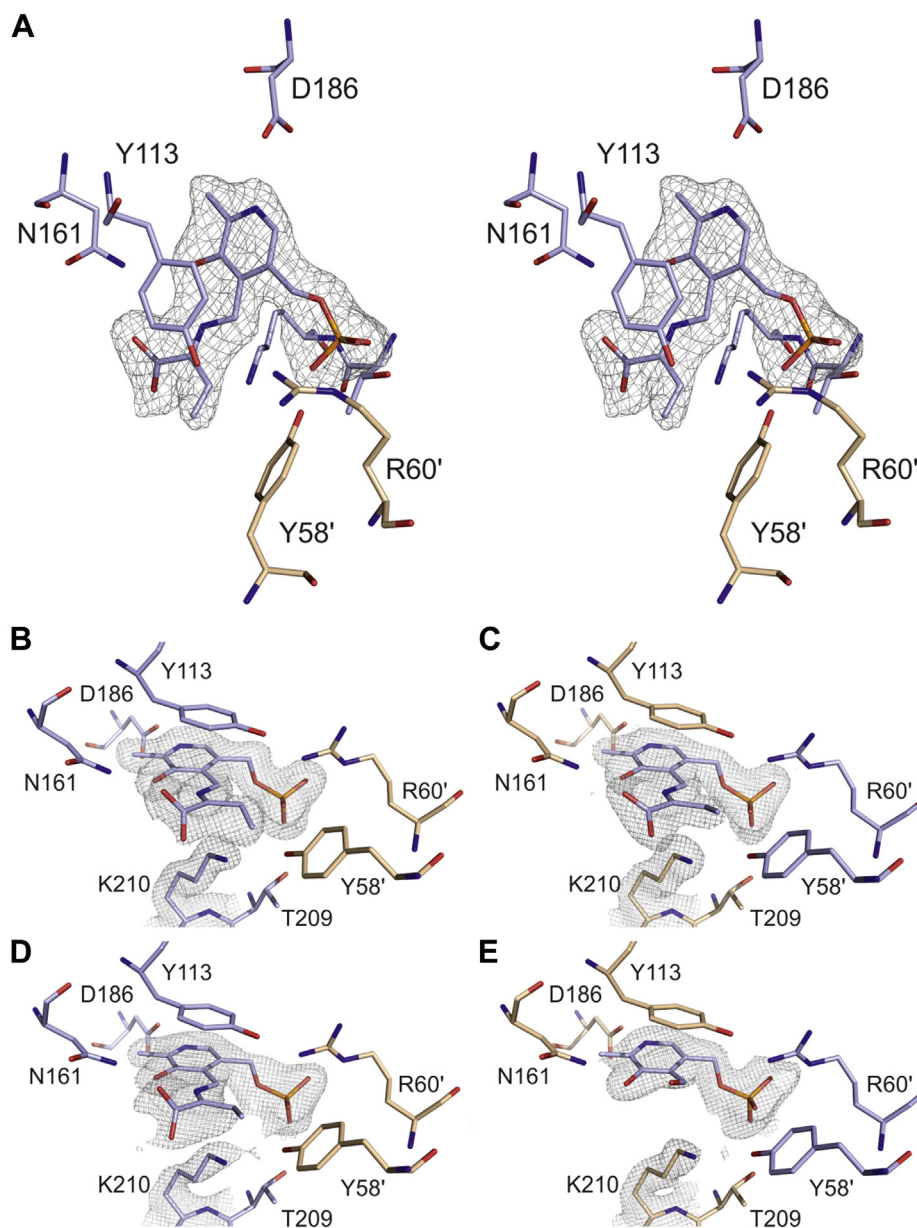


**Figure 4. Electron density maps of PLP in the intermediate-bound form.** A, Fo-Fc Polder OMIT map for PLP in chain A of the homotetramer, contoured at  $4\sigma$  and in wall-eyed stereo view. B–E, 2Fo-Fc maps of PLP in the active sites of the four subunits of the homotetramer (chain A to chain D, respectively). The electron density, contoured at the level of  $1\sigma$ , is shown for Lys210 and PLP derivatives in subunits A–C and for free PLP in subunit D. PLP, pyridoxal 5'-phosphate.

consistent with having observed this ketimine intermediate in chains A–C of *Tm*MetY (albeit after elimination of acetate from L-OAHS). That is, soaking the crystal with L-OAHS led to transaldimination and the reaction proceeded to the point of the  $\beta,\gamma$ -unsaturated ketimine (Fig. 5). However, in the absence of  $\text{HS}^-$ , the reaction could not go to completion and a stable intermediate (5 in Fig. 5) was observed in the active site. In addition to the formation of the external aldimine with PLP, the carboxylate of this intermediate is anchored in place *via* a salt bridge with the side chain of Arg405. As expected after the elimination of acetate, the  $\text{C}\beta$  and  $\text{C}\gamma$  atoms of the intermediate are accommodated in a relatively spacious pocket. The nearest neighbors are the side chains of Lys210 and Tyr58'

(Fig. 4), which are at distances of 3.1 Å and 3.4 Å, respectively, from  $\text{C}\gamma$ .

Our structure is the first to capture the  $\beta,\gamma$ -unsaturated ketimine intermediate that MetY has in common with MetB. In MetB, the absence of the second substrate (L-cysteine) results in an enzyme-catalyzed elimination in which the ketimine is converted to an external aldimine of aminocrotonate, and then to  $\alpha$ -ketobutyrate and  $\text{NH}_3$  (28–30). Although somewhat indirect, we are confident our structure contains the ketimine because the aminocrotonate–PLP adduct would have caused a change in color of the yellow crystals (28, 55). Moreover, several studies have tested MetY enzymes for  $\gamma$ -elimination activity (*i.e.*, the formation of  $\alpha$ -ketobutyrate) and failed to

## Structure and function of *Thermotoga maritima* MetY

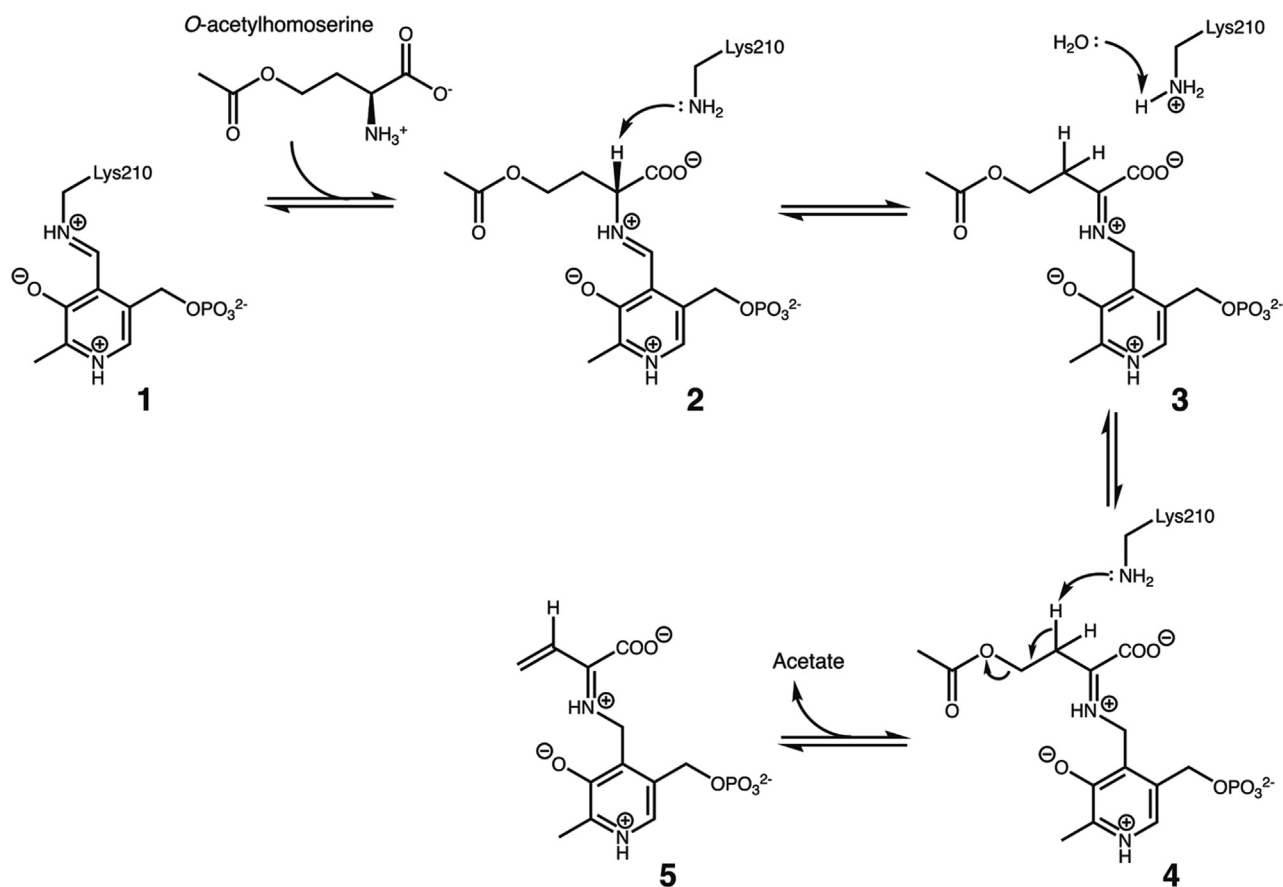


**Figure 5. Scheme for the MetY-catalyzed  $\gamma$ -elimination of acetate from L-OAHS.** The scheme follows that established for the *Escherichia coli* cystathionine  $\gamma$ -synthase, *EcMetB* (28–30). Elimination of acetate yields the  $\beta,\gamma$ -unsaturated ketimine intermediate (5) that we observed in the active site of *TmMetY*. Resonance structures and the quinonoid intermediate between (2) and (3) have been omitted for clarity. L-OAHS, L-O-acetylhomoserine; MetY, O-acetylhomoserine aminocarboxylpropyltransferase; *TmMetY*, *Thermotoga maritima* MetY.

detect it (21, 22, 41, 46). Our serendipitous discovery provides further evidence that MetY does not catalyze  $\gamma$ -elimination in the absence of  $\text{HS}^-$ , as the ketimine intermediate has proven stable enough to capture crystallographically.

### Insights into substrate specificity

When comparing MetB and *TmMetY*, two features of substrate specificity in the latter are (1) its strong preference for L-OAHS over L-OSHS (Table 1) and (2) its inability to accept L-cysteine as the second substrate (33). Our structural analyses provide explanations for both these distinguishing properties of *TmMetY*.

To investigate the structural basis of acylhomoserine specificity, we first soaked *TmMetY* crystals with L-OSHS. However, this proved unsuccessful. Either the crystals dissolved before they could be collected and frozen or those that were able to be collected were visibly fractured and produced only poor-quality diffraction. Accommodating the larger substrate appeared to require too much movement within the structure, leading to disintegration of the crystal lattice.

Next, we used AutoDock Vina (56) to model the L-OAHS and L-OSHS external aldimine complexes (*i.e.*, intermediate 2 in Fig. 5 and the equivalent where the acetyl moiety is replaced by a succinyl group). We designated a maximum of five

possible orientations, and these were readily generated for PLP–OAHS. However, only three possible docked orientations could be generated for PLP–OSHS. Visual inspection indicated that for both ligands, all but the highest scoring models could be disregarded because of highly improbable orientations of the PLP. The binding energies calculated for the highest scoring orientations were  $-9.1 \text{ kcal mol}^{-1}$  and  $-8.4 \text{ kcal mol}^{-1}$ , for PLP–OAHS and PLP–OSHS, respectively. These energies implied that each substrate could indeed be accommodated in the active site and are consistent with our finding that the  $K_M^{\text{APP}}$  values for each substrate (Table 1) are comparable with one another.

The results of the docking are shown in Figure 6 and in wall-eyed stereo in Fig. S5. The acetyl group of PLP–OAHS, missing from our structure with the ketimine intermediate, fits snugly into a pocket created by Arg60', Arg270', Ile61', and Tyr58' (Fig. 6, B, D and E). In the model, the carbonyl oxygen of the acetyl group is well positioned to form a hydrogen bond with a guanidino nitrogen of Arg60' (modeled O–N distance of 3.0 Å). The bulkier succinyl group of PLP–OSHS was also docked into this pocket but only in a torsionally constrained conformation, which was required to minimize clashes and too-close contacts with the arginine residues (Fig. 6, C–E). Nevertheless, our modeling suggests that a carboxylate oxygen



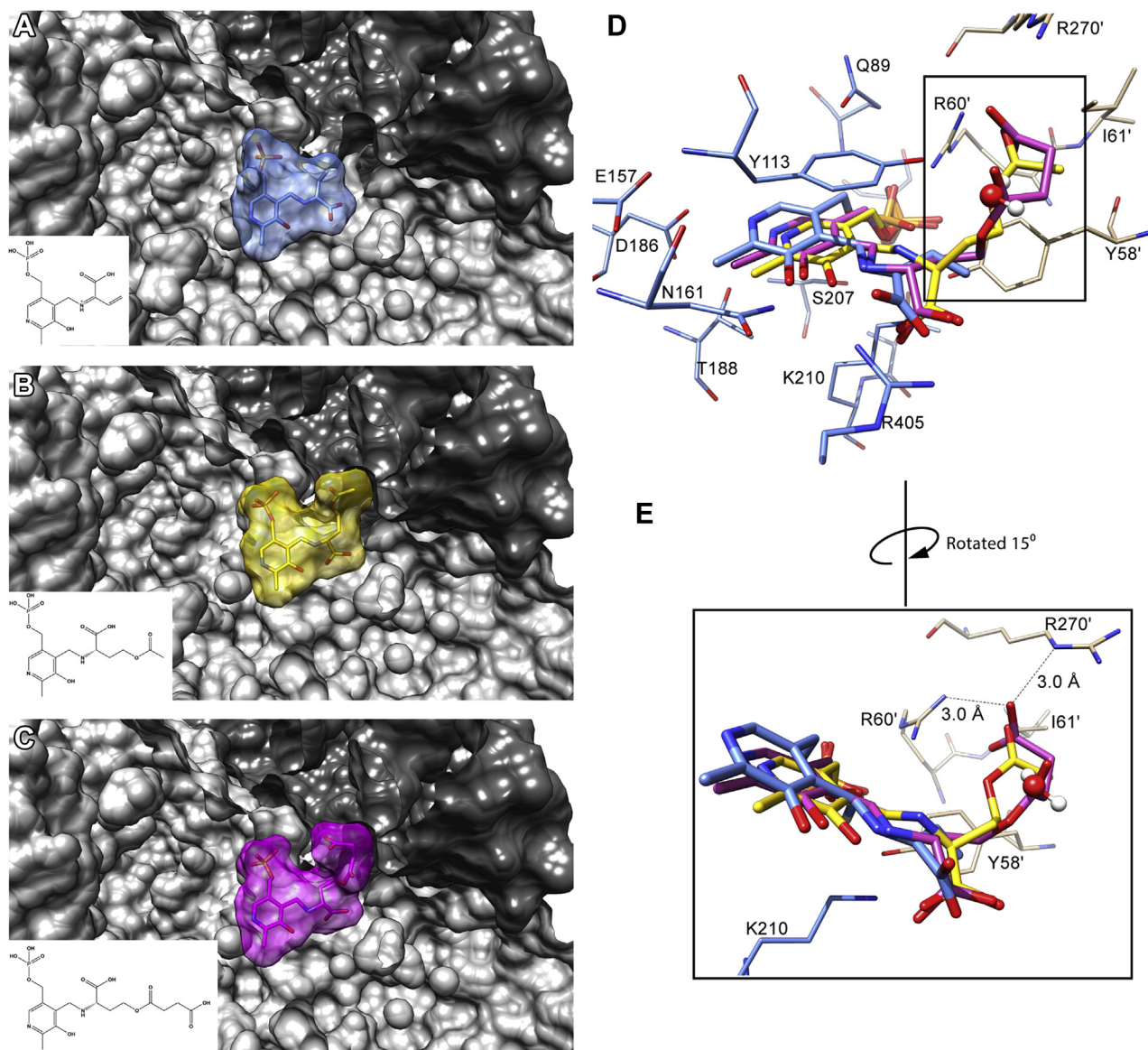


**Figure 6. Modeling of PLP-OAHS and PLP-OSHS into the active site of the intermediate-bound *TmMetY* structure (PDB ID: 7KB1).** A, the crystal structure of the PLP-ketimine intermediate complex (blue). B, PLP-OAHS (yellow) and C, PLP-OSHS (magenta) are docked into the active site. Subunit A is shown in light gray and subunit B in dark gray, with stick diagrams of each PLP complex inset. D, residues lining the active site pocket, with colors of the PLP adducts matching those in panels A–C. E, close-up of the pocket formed by Arg60', Arg270', Ile61', and Tyr58', coordinating the distal end of the acyl-homoserine substrate. Selected distances are indicated. A solvent molecule is shown in red and white spheres in panels D and E. Modeling was performed with AutoDock Vina as a plugin of UCSF Chimera. OAHS, O-acetylhomoserine; PLP, pyridoxal 5'-phosphate; *TmMetY*, *Thermotoga maritima* MetY.

of the succinyl moiety could form a salt bridge and/or hydrogen bonds with one or both of the arginine side chains (Fig. 6E).

The contortion required to accommodate L-OSHS also places the carbonyl group of the succinyl moiety directly atop an active site water that was resolved in our intermediate-bound structure (water #27). This is the closest water molecule to Lys210 in the structure. Therefore, it is a candidate to accept a proton from the side chain of Lys210, after this residue has deprotonated the external aldimine to form 3 in Figure 5. The poor turnover of *TmMetY* with L-OSHS as a substrate may be, in part, because even when it does bind productively, it occludes this water molecule from the active site.

Unlike *TmMetY*, *EcMetB* prefers L-OSHS as a substrate (30), although supplementing an *E. coli* growth medium with L-OAHS has shown that *EcMetB* can use this substrate when the cell lacks an endogenous source of L-OSHS (18). Although Arg60' is conserved in the two enzymes (Arg48' in *EcMetB*), it is noteworthy that Arg270' in *TmMetY* is replaced by a much smaller asparagine residue (Asn227'). Ile61' is replaced by Arg49' in *EcMetB* but with the side chain oriented away from the substrate. These differences serve to create space for the succinyl group of L-OSHS by opening out the walls of the *EcMetB* active site.

Crystallization experiments and X-ray data collection have been reported for MetB from the bacterial pathogen of rice, *Xanthomonas oryzae* pv. *oryzae* (57). During the preparation of

## Structure and function of *Thermotoga maritima* MetY

our article, three unpublished structures of this enzyme (*XoMetB*) became available in the PDB. Of most relevance, one structure (PDB ID: 6LD8) successfully captured a PLP–aminoacrylate adduct and the second substrate, L-cysteine, together in the active site (Fig. 7). This *XoMetB* structure (58) confirms the pattern observed for *EcMetB*. Arg60' in *TmMetY* is conserved (Arg56' in *XoMetB*), but Arg270' is replaced by Asn235', and Ile61' is replaced by a less bulky serine residue (Ser57'). Although no functional data have been reported yet, the absence of an arginine equivalent to Arg270' strongly suggests the enzyme will utilize L-OSHS and not L-OAHS as its first substrate.

By capturing L-cysteine in the active site, the *XoMetB* structure also sheds light on the strict specificity of *TmMetY* for HS<sup>-</sup> (rather than L-cysteine). In *XoMetB*, every functional group of L-cysteine makes favorable interactions with the enzyme (Fig. 7). Most obviously, the side chain of Arg114 is perfectly positioned to make a salt bridge with the cysteine carboxylate. *TmMetY* has Asn118 in the equivalent position, which would be too distant to interact with a bound cysteine. On the other hand, the need for *XoMetB* to have Asn235', instead of Arg270' in *TmMetY*, also becomes clear. Its side chain nitrogen is within hydrogen bonding distance of the

cysteine carboxylate, albeit at 3.5 Å. Importantly, however, an arginine in this position would make too-close contacts of less than 2 Å with an incoming cysteine. The other substrate-binding residues that differ between *XoMetB* and *TmMetY* are Glu333, which participates in two hydrogen bonds with L-cysteine but is replaced with an alanine in *TmMetY*, and Asp53', which makes one hydrogen bond but is replaced with an isoleucine. The only conserved residues in the L-cysteine binding site of *XoMetB* are Tyr109 (Tyr113 in *TmMetY*) and Arg56' (Arg60' in *TmMetY*; Fig. 7). The picture that emerges is the one in which *TmMetY* cannot accept L-cysteine as a substrate because of the steric clash with Arg270' and the lack of favorable interactions elsewhere in the active site.

The PLP–aminoacrylate adduct in the active site of *XoMetB* is an intermediate in the reactions catalyzed by cystathionine β-synthase (28, 55) and cystathionine β-lyase (51, 52). It has one less carbon than the ketimine intermediate in our *TmMetY* structure. By superimposing the two structures (Fig. 7), it becomes apparent that the nucleophilic thiol group of L-cysteine is well positioned to attack the β,γ-unsaturated ketimine intermediate, as expected from mechanistic studies (28, 29). Furthermore, water #27 in the *TmMetY* structure occupies the same position as the cysteine thiol in *XoMetB*. It forms a hydrogen bond of 2.7 Å with the side-chain hydroxyl of Tyr113. Regardless of its putative role at earlier steps in the catalytic cycle, this water must be displaced by the incoming second substrate, HS<sup>-</sup>, as it effects its nucleophilic attack on the ketimine.

### Concluding remarks

Jacques Monod's famous axiom is that “anything found to be true of *E. coli* must also be true of elephants” (59). Unfortunately, this is not the case for methionine biosynthesis. Recent studies underpinned by bacterial phylogenetics have confirmed that the *E. coli* pathway, starting from succinyl-CoA and proceeding *via trans*-sulfurylation (Fig. 1), is a comparatively uncommon biosynthetic route to methionine (3, 9). In this work, we have shed new light on MetY, the predominant sulfurylation enzyme in bacterial methionine biosynthesis.

We have shown the *T. maritima* MetY to be thermostable and to catalyze the formation of homocysteine from L-OAHS and bisulfide with high efficiency ( $k_{\text{cat}}^{\text{APP}}/K_{\text{M}}^{\text{APP}} = 1 \times 10^5 \text{ s}^{-1} \text{ M}^{-1}$ ). A direct sulfurylation pathway with HS<sup>-</sup> as the sulfur donor is consistent with the ecological niche of *T. maritima*. The bacterium is widespread in sedimentary marine environments around geothermal vents (39), which are sources of dissolved hydrogen sulfide gas (60). *TmMetY* was also able to accept L-OSHS as a substrate, albeit with a 1000-fold reduction in catalytic efficiency. By solving the structure of *TmMetY*, we revealed Arg270 as a particularly critical determinant of substrate specificity: it helps in walling off the active site to disfavor the binding of the bulkier L-OSHS (Fig. 6), and it prevents L-cysteine from acting as the second substrate (Fig. 7). Mutagenesis of this residue may provide insights into specificity, and also into the proposed evolution of MetB from an ancestral MetY (18).

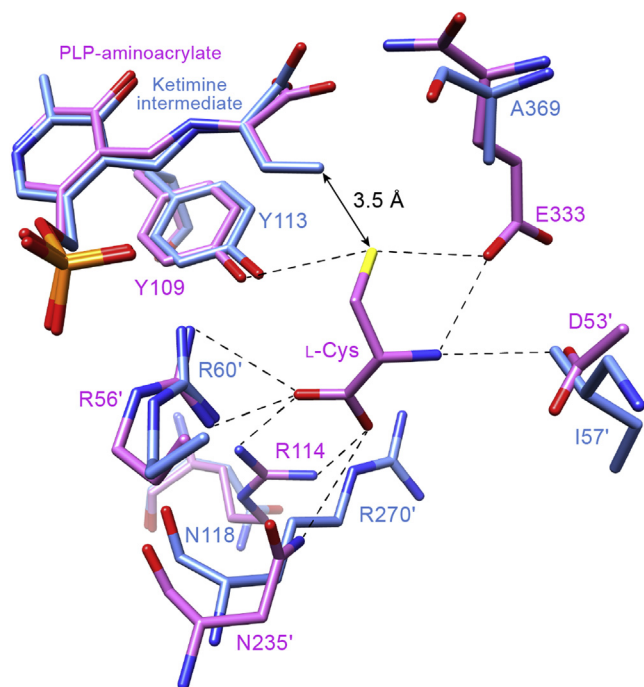


**Figure 7. Superposition of select active site residues in the intermediate-bound structures of *TmMetY* (blue; PDB ID: 7KB1) and *XoMetB* (magenta; PDB ID: 6LD8).** The PLP–aminoacrylate adduct from *XoMetB* overlays the β,γ-unsaturated ketimine intermediate in *TmMetY*. Hydrogen bonds and the salt bridge between *XoMetB* and its substrate, L-cysteine, are shown as dashed black lines. Distances are omitted for clarity, but all are between 2.7 Å and 3.5 Å. These distances vary slightly between active sites in the *XoMetB* homotetramer; shown is the active site formed by chains B and C. In the course of the γ-replacement reaction, the thiol group of L-cysteine (in *XoMetB*), or free HS<sup>-</sup> (in *TmMetY*), makes a nucleophilic attack on the γ-carbon of the β,γ-unsaturated ketimine. The relevant distance from the superposition (3.5 Å) is indicated with a doubled-headed black arrow. PDB, Protein Data Bank; PLP, pyridoxal 5'-phosphate; *TmMetY*, *Thermotoga maritima* MetY.

Our structural studies also fortuitously captured the  $\beta,\gamma$ -unsaturated ketimine reaction intermediate in the active site (Fig. 4). This intermediate is identical in the catalytic cycles of MetY and MetB although it has not been observed in the latter enzyme because in the absence of a second substrate, it is eliminated to yield  $\alpha$ -ketobutyrate and ammonia (28–30). It is not clear from our study what prevents the elimination reaction in *Tm*MetY, although this activity has never been observed for any MetY (21, 22, 41, 46).

Overall, this work reiterates the subtle structural mechanisms by which homologous PLP-dependent enzymes can effect different catalytic outcomes (13, 16, 27). It also emphasizes the value to be gained from venturing beyond well-studied model organisms for investigating the diverse enzymology in the biosphere (9, 61–63).

## Experimental procedures

### Cloning and mutagenesis

The expression vector for MetY from *T. maritima* strain MSB8 (NCBI locus tag THEMA\_RS00225) was purchased from the DNASU Plasmid Repository (<https://biodesign.asu.edu/personalized-diagnostics/dnasu-plasmid-repository>). This pMH series plasmid was originally constructed by the Joint Consortium for Structural Genomics (64). It included an N-terminal His<sub>6</sub>-tag and the *araC* ORF for arabinose-inducible expression. DNA sequencing of the plasmid revealed that it had a 1-bp deletion mutation within the sequence encoding the His<sub>6</sub>-tag, resulting in a –1 frameshift. The frameshift was corrected by site-directed mutagenesis using forward primer 5' TCA TCA TCA CAT GGA CTG GAA GAA ATA CGG TTA CAA CAC AAG GGC 3' and reverse primer 5' CCA GTC CAT GTG ATG ATG ATG ATG AAT TTT ATC AGA TCC CAT GGG T 3' by the method of Liu and Naismith (65). Plasmid DNA was used to transform *E. coli* cloning strain E. cloni 10G (Lucigen) and then the *E. coli* expression strain LMG194 (Invitrogen). Correction of the mutation was confirmed by DNA sequencing.

### Protein expression and purification

*E. coli* cultures were grown at 37 °C in phosphate-buffered Terrific Broth (Formedium) supplemented with 0.1 mg ml<sup>-1</sup> ampicillin, to an absorbance at 600 nm of 0.6, before induction of protein expression by the addition of 0.2% arabinose (GoldBio). The incubation temperature was decreased to 28 °C, and cultures were incubated for a further ~12 to 16 h. Cells were harvested by centrifugation and resuspended in the lysis buffer [50 mM potassium phosphate, 300 mM sodium chloride, 10% (v/v) glycerol, 4  $\mu$ l ml<sup>-1</sup> protease inhibitor cocktail (Sigma), 0.5 mg ml<sup>-1</sup> egg white lysosome (GoldBio) and 5 U ml<sup>-1</sup> benzonase nuclease (Merck), pH 7.5]. Cells were lysed by sonication on ice, which was followed by centrifugation to separate soluble protein from cellular debris.

Soluble protein was purified by immobilized metal ion affinity chromatography. Clarified cell lysate was filtered through a 0.45- $\mu$ m sterile syringe-driven filter and then applied to

Talon cobalt resin (Clontech) pre-equilibrated with the lysis buffer, and incubated at 4 °C with tumbling for 30 min. The protein-bound resin was then pelleted by centrifugation and washed twice with the lysis buffer to remove unbound protein. The resin was transferred to a Poly-Prep gravity flow column (Bio-Rad), and protein was eluted with the lysis buffer containing 150-mM imidazole. Visibly yellow fractions were pooled and injected onto a HiPrep 26/10 desalting column pre-equilibrated with the storage buffer [50 mM potassium phosphate, 200 mM sodium chloride, 10% (v/v) glycerol, pH 7.5]. The eluted protein was concentrated with a 10-kDa molecular weight cut-off centrifugal concentrator (EMD Millipore). The protein subunit concentration was calculated from  $A_{280\text{nm}}$  measurements using the specific extinction coefficient of 44,810 l mol<sup>-1</sup> cm<sup>-1</sup>, as calculated by ExpASY ProtParam (66). The purity of the protein was evaluated as  $\geq 95\%$  by SDS-PAGE.

### Fluorescence thermal shift assay

The melting temperature of *Tm*MetY was determined by the fluorescence thermal shift assay. Assays in a total volume of 20  $\mu$ l were set up in 96-well plates (LightCycler 480 multiwell, Roche Diagnostics) and contained 50-mM HEPES, pH 7.0, 5 $\times$  Sypro Orange (Life Technologies) and 20  $\mu$ M *Tm*MetY. The plate was covered with LightCycler 480 sealing film (Roche Diagnostics) and centrifuged at 1000g for 1 min. The fluorescence was monitored over the range of 20 to 95 °C (ramp of 1.2 °C min<sup>-1</sup>) in a LightCycler 480 (Roche). The melting temperature was determined from the first derivative of the fluorescence data (-dF/dt) calculated in Exor 4.0 LightCycler Software (Roche Diagnostics). The assay was performed for two biological replicates (protein batches independently cultured and purified), with technical triplicates for each.

### Homocysteine assay

Our synthesis of the substrate L-OAHS, which was used in activity assays, was reported previously (33). The conditions of the primary end-point assay were optimized so that the rate of reaction was linear over the incubation period. The reactions contained 50 mM HEPES, pH 7.0, 10  $\mu$ M PLP, and 5 mM sodium sulfide to provide excess HS<sup>-</sup>, as well as varying concentrations of the primary substrate L-OAHS or L-OSHS between 0 and 10 mM (with 0.25 mM being the lowest substrate concentration used). *Tm*MetY concentrations of 0.5 nM or 2  $\mu$ M were used for L-OAHS and L-OSHS assays, respectively. The reaction was incubated at 70 °C (unless otherwise stated) for 3 min before increasing the temperature to 95 °C for a further 5 min, to denature the protein and stop the reaction. Under these conditions, approximately 1% of the substrate was converted to the product, ensuring that initial rates of reaction ( $v_0$ ) were being estimated in assays at each substrate concentration.

The secondary reaction for L-homocysteine quantitation (Fig. S1) was performed at 37 °C in a Cary 100 UV-Vis spectrophotometer (Agilent Technologies), using the

## Structure and function of *Thermotoga maritima* MetY

Homocysteine Enzymatic Assay Kit (Diazyme Laboratories). A 10- $\mu$ l aliquot of the standard or reaction mixture was added to 150  $\mu$ l of reagent 1 in a quartz cuvette, and the spectrophotometer was zeroed at 340 nm. After 1 min, 25  $\mu$ l of reagent 2 was added and mixed by pipetting. At 5 min, 15  $\mu$ l of reagent 3 was added and mixed by pipetting. The decrease in absorbance at 340 nm was monitored spectrophotometrically (67), and the linear rate of reaction in  $\text{nmol min}^{-1}$  was calculated between 7 and 10 min. A standard curve of the rate of reaction *versus* the concentration of an L-homocysteine standard (Sigma) was linear for L-homocysteine amounts between 0.01 and 0.5 nmol. We discovered that L-homocysteine was somewhat unstable at high temperatures, so the L-homocysteine standards were subjected to the same high temperature incubation steps of the primary end-point reaction before the secondary reaction.

### Crystal growth

For crystallization experiments, affinity-purified *Tm*MetY was injected onto a 16/60 S200 Superdex column (GE Healthcare) equilibrated with the crystallization buffer (100 mM Tris HCl, pH 8.0). Fractions corresponding to the central portion of the elution peak were pooled and concentrated by a centrifugal concentrator. Commercial crystallization screens were used to find conditions for crystal growth. Sitting-drop vapor diffusion screens were set up in 3-well plates (Hampton Research) using a mosquito LCP (SPT Labtech) with a 1:1 ratio of protein to well solution and final protein concentrations of 5  $\text{mg ml}^{-1}$ , 2.5  $\text{mg ml}^{-1}$ , and 1.25  $\text{mg ml}^{-1}$ . Plates were incubated at 16 °C and imaged using a Rock Imager crystal hotel (Formulatrix Inc). Small, star-shaped, yellow crystal clusters formed within 1 to 3 weeks in several conditions of the Morpheus HT screen (Molecular Dimensions). Fine screening and microseeding resulted in diffraction quality crystals that formed in 0.1 M Bis Tris, pH 5.4, 0.2 M  $\text{MgCl}_2$ , and 17 to 20% PEG 3350, with a final protein concentration of 1.25  $\text{mg ml}^{-1}$ . For the intermediate-bound structure, crystals were transferred to a new drop containing 10 mM L-OAHS for 24 h before cryo-freezing.

### X-ray data collection and processing

Single crystals were flash-frozen in liquid nitrogen with the well solution acting as a cryoprotectant. X-ray diffraction data were collected on the MX2 beamline at the Australian Synchrotron (68). Datasets were collected at 100 K and a wavelength of 0.9357 Å (13 keV). Diffraction data were processed by the XDS package (69) and its graphical user interface, XDSGUI. Dataset cutoff was chosen based on  $\text{CC}_{1/2}$  statistics and completeness in the highest resolution shell higher than 70%. The structure of the internal aldimine form (PDB ID: 7KB0) was solved by molecular replacement with cystathionine  $\beta$ -lyase from *T. maritima* as a template (undeposited structure, 31.7% amino acid sequence identity), using the Phenix package (70). The resulting model was rebuilt in Coot (71). The intermediate-bound structure (PDB ID: 7KB1) was solved by molecular replacement using the internal aldimine structure as a template. The co-ordinates for the ligand in the

active site were generated by the National Cancer Institute (USA) web server (<https://cactus.nci.nih.gov/translate/>), from which the crystallographic information file was generated in Phenix. Structural refinement was performed using phenix.refine of the Phenix package.

### Modeling of external aldimine states

The co-ordinates for PLP covalently bound to L-OAHS and L-OSHS were generated using the National Cancer Institute (USA) web server (<https://cactus.nci.nih.gov/translate/>). The molecules were then modeled into our intermediate-bound structure (7KB1), from which the ligand had been removed, using AutoDock Vina (56). Default fitting parameters were used to generate up to five potential orientations for each molecule within the active site. However, through visual inspection of the results, all but one of the possible solutions for each molecule could be easily disregarded because of highly improbable orientations of the PLP.

### Data availability

The structures of *T. maritima* MetY have been deposited to the PDB ([www.rcsb.org](http://www.rcsb.org)) with accession codes 7KB0 and 7KB1 for the internal aldimine and intermediate-bound forms, respectively.

---

*Supporting information*—This article contains [supporting information](#).

*Acknowledgments*—We are grateful to Prof Emily Parker (Victoria University of Wellington, New Zealand) for helpful discussions on the mechanism of MetY. This research was undertaken in part using the MX2 beamline at the Australian Synchrotron, part of ANSTO, and made use of the Australian Cancer Research Foundation (ACRF) detector. We thank the New Zealand Synchrotron Group for facilitating access to the MX beamlines.

*Author contributions*—J. L. B. conceptualization, investigation, methodology, formal analysis, visualization, writing—original draft, and writing—review and editing. P. P. formal analysis, visualization, and writing—review and editing. J. L. O. M. investigation and writing—review and editing. M. S. and C. J. S. formal analysis and writing—review and editing. W. M. P. conceptualization, formal analysis, writing—review and editing, supervision, project administration, and funding acquisition.

*Funding and additional information*—This work was supported by a grant from the Marsden Fund (18-VUW-050) and the award of a Rutherford Discovery Fellowship, both to W. M. P.

*Conflict of interest*—The authors declare that they have no conflicts of interest with the contents of this article.

*Abbreviations*—The abbreviations used are: EC, Enzyme Commission; *Ec*MetB, *E. coli* MetB;  $k_{\text{cat}}^{\text{APP}}$ , apparent turnover number;  $K_{\text{M}}^{\text{APP}}$ , apparent Michaelis–Menten constant; L-OAHS, L-O-acetylhomoserine; L-OSHS, L-O-succinylhomoserine; MetB, cystathionine  $\gamma$ -synthase; MetY, O-acetylhomoserine aminocarboxylpropyltransferase; PDB, Protein Data Bank; PLP,

pyridoxal 5'-phosphate; *Tm*MetY, *Thermotoga maritima* MetY;  $T_{\text{opt}}$  optimal temperature.

## References

- Valley, C. C., Cembran, A., Perlmutter, J. D., Lewis, A. K., Labello, N. P., Gao, J., and Sachs, J. N. (2012) The methionine-aromatic motif plays a unique role in stabilizing protein structure. *J. Biol. Chem.* **287**, 34979–34991
- Aledo, J. C. (2019) Methionine in proteins: The Cinderella of the proteinogenic amino acids. *Protein Sci.* **28**, 1785–1796
- Ferla, M. P., and Patrick, W. M. (2014) Bacterial methionine biosynthesis. *Microbiology* **160**, 1571–1584
- Hesse, H., Kreft, O., Maimann, S., Zeh, M., and Hoefgen, R. (2004) Current understanding of the regulation of methionine biosynthesis in plants. *J. Exp. Bot.* **55**, 1799–1808
- Ravanel, S., Gakiere, B., Job, D., and Douce, R. (1998) The specific features of methionine biosynthesis and metabolism in plants. *Proc. Natl. Acad. Sci. U. S. A.* **95**, 7805–7812
- Rowbury, R. J. (1964) Synthesis of cystathionine and its control in *Salmonella typhimurium*. *Nature* **203**, 977–978
- Rowbury, R. J., and Woods, D. D. (1964) *O*-Succinylhomoserine as an intermediate in the synthesis of cystathionine by *Escherichia coli*. *J. Gen. Microbiol.* **36**, 341–358
- Smith, D. A., and Childs, J. D. (1966) Methionine genes and enzymes of *Salmonella typhimurium*. *Hereditas* **21**, 265–286
- Bastard, K., Perret, A., Mariage, A., Bessonnet, T., Pinet-Turpault, A., Petit, J. L., Darii, E., Bazire, P., Vergne-Vaxelaire, C., Brewce, C., Debard, A., Pellouin, V., Besnard-Gonnet, M., Artiguenave, F., Médigue, C., et al. (2017) Parallel evolution of non-homologous isofunctional enzymes in methionine biosynthesis. *Nat. Chem. Biol.* **13**, 858–866
- Berney, M., Berney-Meyer, L., Wong, K. W., Chen, B., Chen, M., Kim, J., Wang, J., Harris, D., Parkhill, J., Chan, J., Wang, F., and Jacobs, W. R., Jr. (2015) Essential roles of methionine and *S*-adenosylmethionine in the autarkic lifestyle of *Mycobacterium tuberculosis*. *Proc. Natl. Acad. Sci. U. S. A.* **112**, 10008–10013
- Chaton, C. T., Rodriguez, E. S., Reed, R. W., Li, J., Kenner, C. W., and Korotkov, K. V. (2019) Structural analysis of mycobacterial homoserine transacetylases central to methionine biosynthesis reveals druggable active site. *Sci. Rep.* **9**, 20267
- Liang, J., Han, Q., Tan, Y., Ding, H., and Li, J. (2019) Current advances on structure-function relationships of pyridoxal 5'-phosphate-dependent enzymes. *Front. Mol. Biosci.* **6**, 4
- Toney, M. D. (2011) Controlling reaction specificity in pyridoxal phosphate enzymes. *Biochim. Biophys. Acta* **1814**, 1407–1418
- Raboni, S., Spyarakis, F., Campanini, B., Amadasi, A., Bettati, S., Peracchi, A., Mozzarelli, A., and Contestabile, R. (2010) Pyridoxal 5'-phosphate-dependent enzymes: Catalysis, conformation, and genomics. In *Comprehensive Natural Products II: Chemistry and Biology*, Elsevier Ltd, New York, NY: 273–350
- Richard, J. P., Amyes, T. L., Crugeiras, J., and Rios, A. (2009) Pyridoxal 5'-phosphate: Electrophilic catalyst extraordinaire. *Curr. Opin. Chem. Biol.* **13**, 475–483
- Eliot, A. C., and Kirsch, J. F. (2004) Pyridoxal phosphate enzymes: Mechanistic, structural, and evolutionary considerations. *Annu. Rev. Biochem.* **73**, 383–415
- Mitchell, A. L., Attwood, T. K., Babbitt, P. C., Blum, M., Bork, P., Bridge, A., Brown, S. D., Chang, H. Y., El-Gebali, S., Fraser, M. I., Gough, J., Haft, D. R., Huang, H., Letunic, I., Lopez, R., et al. (2019) InterPro in 2019: Improving coverage, classification and access to protein sequence annotations. *Nucleic Acids Res.* **47**, D351–D360
- Hacham, Y., Gophna, U., and Amir, R. (2003) *In vivo* analysis of various substrates utilized by cystathionine  $\gamma$ -synthase and *O*-acetylhomoserine sulfhydrylase in methionine biosynthesis. *Mol. Biol. Evol.* **20**, 1513–1520
- Jeske, L., Placzek, S., Schomburg, I., Chang, A., and Schomburg, D. (2019) BRENDA in 2019: A European ELIXIR core data resource. *Nucleic Acids Res.* **47**, D542–D549
- Hwang, B. J., Park, S. D., Kim, Y., Kim, P., and Lee, H. S. (2007) Biochemical analysis on the parallel pathways of methionine biosynthesis in *Corynebacterium glutamicum*. *J. Microbiol. Biotechnol.* **17**, 1010–1017
- Kulikova, V. V., Revtovich, S. V., Bazhulina, N. P., Anufrieva, N. V., Kotlov, M. I., Koval, V. S., Morozova, E. A., Hayashi, H., Belyi, Y. F., and Demidkina, T. V. (2019) Identification of *O*-acetylhomoserine sulfhydrylase, a putative enzyme responsible for methionine biosynthesis in *Clostridioides difficile*: Gene cloning and biochemical characterizations. *IUBMB Life* **71**, 1815–1823
- Kulikova, V. V., Anufrieva, N. V., Kotlov, M. I., Morozova, E. A., Koval, V. S., Belyi, Y. F., Revtovich, S. V., and Demidkina, T. V. (2021) *O*-acetylhomoserine sulfhydrylase from *Clostridium novyi*. Cloning, expression of the gene and characterization of the enzyme. *Protein Expr. Purif.* **180**, 105810
- Tran, T. H., Krishnamoorthy, K., Begley, T. P., and Ealick, S. E. (2011) A novel mechanism of sulfur transfer catalyzed by *O*-acetylhomoserine sulfhydrylase in the methionine-biosynthetic pathway of *Wolinella succinogenes*. *Acta Crystallogr. D Biol. Crystallogr.* **67**, 831–838
- Imagawa, T., Utsunomiya, H., Tsuge, H., Ebihara, A., Kanagawa, M., Nakagawa, N., Kuroishi, C., Agari, Y., Kuramitsu, S., and Yokoyama, S. (2007) PDB ID 2CBI: Crystal structure of *O*-acetyl homoserine sulfhydrylase from *Thermus thermophilus* HB8, OAH2. <https://doi.org/10.2210/pdb2212CB2211/pdb>
- Imagawa, T., Kousumi, Y., Tsuge, H., Utsunomiya, H., Ebihara, A., Nakagawa, N., Yokoyama, S., Kuramitsu, S., and RIKEN Structural Genomics/Proteomics Initiative (2005) PDB ID 2CTZ: Crystal structure of *O*-acetyl homoserine sulfhydrylase from *Thermus thermophilus* HB8. <https://doi.org/10.2210/pdb2212CTZ/pdb>
- Halavaty, A. S., Brunzelle, J. S., Wawrzak, Z., Onopriyenko, O., Savchenko, A., Anderson, W. F., and Center for Structural Genomics of Infectious Diseases (2014) PDB ID 4OC9: 2.35 Å resolution crystal structure of putative *O*-acetylhomoserine (thiol)-lyase (MetY) from *Campylobacter jejuni* subsp. *jejuni* NCTC 11168 with *N*'-pyridoxyl-lysine-5'-monophosphate at position 205. <https://doi.org/10.2210/pdb2214OC2219/pdb>
- Aitken, S. M., Lodha, P. H., and Morneau, D. J. (2011) The enzymes of the transsulfuration pathways: Active-site characterizations. *Biochim. Biophys. Acta* **1814**, 1511–1517
- Aitken, S. M., and Kirsch, J. F. (2005) The enzymology of cystathionine biosynthesis: Strategies for the control of substrate and reaction specificity. *Arch. Biochem. Biophys.* **433**, 166–175
- Brzovic, P., Holbrook, E. L., Greene, R. C., and Dunn, M. F. (1990) Reaction mechanism of *Escherichia coli* cystathionine  $\gamma$ -synthase: Direct evidence for a pyridoxamine derivative of vinylglyoxylate as a key intermediate in pyridoxal phosphate dependent  $\gamma$ -elimination and  $\gamma$ -replacement reactions. *Biochemistry* **29**, 442–451
- Aitken, S. M., Kim, D. H., and Kirsch, J. F. (2003) *Escherichia coli* cystathionine  $\gamma$ -synthase does not obey ping-pong kinetics. Novel continuous assays for the elimination and substitution reactions. *Biochemistry* **42**, 11297–11306
- Clausen, T., Huber, R., Prade, L., Wahl, M. C., and Messerschmidt, A. (1998) Crystal structure of *Escherichia coli* cystathionine  $\gamma$ -synthase at 1.5 Å resolution. *EMBO J.* **17**, 6827–6838
- Messerschmidt, A., Worbs, M., Steegborn, C., Wahl, M. C., Huber, R., Laber, B., and Clausen, T. (2003) Determinants of enzymatic specificity in the Cys-Met-metabolism PLP-dependent enzymes family: Crystal structure of cystathionine  $\gamma$ -lyase from yeast and intrafamilial structure comparison. *Biol. Chem.* **384**, 373–386
- Ferla, M. P., Brewster, J. L., Hall, K. R., Evans, G. B., and Patrick, W. M. (2017) Primordial-like enzymes from bacteria with reduced genomes. *Mol. Microbiol.* **105**, 508–524
- Ellman, G. L., Courtney, K. D., Andres, V., and Featherstone, R. M. (1961) A new and rapid colorimetric determination of acetylcholinesterase activity. *Biochem. Pharmacol.* **7**, 88–95
- Frick, B., Schröcksnadel, K., Neurauter, G., Wirleitner, B., Artner-Dworzak, E., and Fuchs, D. (2003) Rapid measurement of total plasma homocysteine by HPLC. *Clin. Chim. Acta* **331**, 19–23

## Structure and function of *Thermotoga maritima* MetY

36. Kusmieriek, K., Chwatko, G., Glowacki, R., and Bald, E. (2009) Determination of endogenous thiols and thiol drugs in urine by HPLC with ultraviolet detection. *J. Chromatogr. B Analyt. Technol. Biomed. Life Sci.* **877**, 3300–3308
37. Choi, C. K., and Dong, M. W. (2005) Sample preparation for HPLC analysis of drug products. In: Ahuja, S., Dong, M. W., eds. *Handbook of Pharmaceutical Analysis by HPLC*, Elsevier, Amsterdam, The Netherlands: 123–144
38. Good, N. E., Winget, G. D., Winter, W., Conolloy, T. N., Izawa, S., and Singh, R. M. M. (1966) Hydrogen ion buffers for biological research. *Biochemistry* **5**, 467–477
39. Huber, R., Langworthy, T. A., König, H., Thomm, M., Woese, C. R., Sleytr, U. B., and Stetter, K. O. (1986) *Thermotoga maritima* sp. nov. represents a new genus of unique extremely thermophilic eubacteria growing up to 90°C. *Arch. Microbiol.* **144**, 324–333
40. Wang, Z. W., Tong, W., Wang, Q. H., Bai, X., Chen, Z., Zhao, J. J., Xu, N. Z., and Liu, S. Q. (2012) The temperature dependent proteomic analysis of *Thermotoga maritima*. *PLoS One* **7**, e46463
41. Kerr, D. S. (1971) *O*-acetylhomoserine sulfhydrylase from *Neurospora*. Purification and consideration of its function in homocysteine and methionine synthesis. *J. Biol. Chem.* **246**, 95–102
42. Ozaki, H., and Shio, I. (1982) Methionine biosynthesis in *Brevibacterium flavum*: Properties and essential role of *O*-acetylhomoserine sulfhydrylase. *J. Biochem.* **91**, 1163–1171
43. Shimizu, H., Yamagata, S., Masui, R., Inoue, Y., Shibata, T., Yokoyama, S., Kuramitsu, S., and Iwama, T. (2001) Cloning and overexpression of the *oah1* gene encoding *O*-acetyl-L-homoserine sulfhydrylase of *Thermus thermophilus* HB8 and characterization of the gene product. *Biochim. Biophys. Acta* **1549**, 61–72
44. Yamagata, S. (1984) *O*-acetylhomoserine sulfhydrylase of the fission yeast *Schizosaccharomyces pombe*: Partial purification, characterization, and its probable role in homocysteine biosynthesis. *J. Biochem.* **96**, 1511–1523
45. Iwama, T., Hosokawa, H., Lin, W. M., Shimizu, H., Kawai, K., and Yamagata, S. (2004) Comparative characterization of the *oah2* gene homologous to the *oah1* of *Thermus thermophilus* HB8. *Biosci. Biotechnol. Biochem.* **68**, 1357–1361
46. Omura, H., Ikemoto, M., Kobayashi, M., Shimizu, S., Yoshida, T., and Nagasawa, T. (2003) Purification, characterization and gene cloning of thermostable *O*-acetyl-L-homoserine sulfhydrylase forming  $\gamma$ -cyano- $\alpha$ -aminobutyric acid. *J. Biosci. Bieng.* **96**, 53–58
47. Yamagata, S. (1971) Homocysteine synthesis in yeast. Partial purification and properties of *O*-acetylhomoserine sulfhydrylase. *J. Biochem.* **70**, 1035–1045
48. Goudarzi, M., and Born, T. L. (2006) Purification and characterization of *Thermotoga maritima* homoserine transsuccinylase indicates it is a transacetylase. *Extremophiles* **10**, 469–478
49. Kaplan, M. M., and Flavin, M. (1966) Cystathionine  $\gamma$ -synthetase of *Salmonella*: Structural properties of a new enzyme in bacterial methionine biosynthesis. *J. Biol. Chem.* **241**, 5781–5789
50. Clausen, T., Huber, R., Laber, B., Pohlentz, H. D., and Messerschmidt, A. (1996) Crystal structure of the pyridoxal-5'-phosphate dependent cystathionine  $\beta$ -lyase from *Escherichia coli* at 1.83 Å. *J. Mol. Biol.* **262**, 202–224
51. Soo, V. W. C., Yosaatmadja, Y., Squire, C. J., and Patrick, W. M. (2016) Mechanistic and evolutionary insights from the reciprocal promiscuity of two pyridoxal phosphate-dependent enzymes. *J. Biol. Chem.* **291**, 19873–19887
52. Clausen, T., Huber, R., Messerschmidt, A., Pohlentz, H. D., and Laber, B. (1997) Slow-binding inhibition of *Escherichia coli* cystathionine  $\beta$ -lyase by L-aminoethoxyvinylglycine: A kinetic and X-ray study. *Biochemistry* **36**, 12633–12643
53. Liebschner, D., Afonine, P. V., Moriarty, N. W., Poon, B. K., Sobolev, O. V., Terwilliger, T. C., and Adams, P. D. (2017) Polder maps: Improving OMIT maps by excluding bulk solvent. *Acta Crystallogr. D Struct. Biol.* **73**, 148–157
54. Giardina, G., Paiardini, A., Montioli, R., Cellini, B., Voltattorni, C. B., and Cutruzzola, F. (2017) Radiation damage at the active site of human alanine:glyoxylate aminotransferase reveals that the cofactor position is finely tuned during catalysis. *Sci. Rep.* **7**, 11704
55. Tu, Y., Kreinbring, C. A., Hill, M., Liu, C., Petsko, G. A., McCune, C. D., Berkowitz, D. B., Liu, D., and Ringe, D. (2018) Crystal structures of cystathionine  $\beta$ -synthase from *Saccharomyces cerevisiae*: One enzymatic step at a time. *Biochemistry* **57**, 3134–3145
56. Trott, O., and Olson, A. J. (2010) AutoDock Vina: Improving the speed and accuracy of docking with a new scoring function, efficient optimization, and multithreading. *J. Comput. Chem.* **31**, 455–461
57. Ngo, H. P., Kim, J. K., Kim, S. H., Pham, T. V., Tran, T. H., Nguyen, D. D., Kim, J. G., Chung, S., Ahn, Y. J., and Kang, L. W. (2012) Expression, crystallization and preliminary X-ray crystallographic analysis of cystathionine  $\gamma$ -synthase (XometB) from *Xanthomonas oryzae* pv. *oryzae*. *Acta Crystallogr. Sect. F Struct. Biol. Commun.* **68**, 1515–1517
58. Ngo, H. P. T., Nguyen, T. D. Q., and Kang, L. W. (2020) PDB ID 6LDD: Crystal structure of cystathionine gamma synthase from *Xanthomonas oryzae* pv. *oryzae* in complex with aminoacrylate and cysteine. <https://doi.org/10.2210/pdb2216LD2218/pdb>
59. Monod, J., and Jacob, F. (1961) General conclusions: Teleonomic mechanisms in cellular metabolism, growth, and differentiation. *Cold Spring Harb. Symp. Quant. Biol.* **26**, 389–401
60. Zierenberg, R. A., Adams, M. W. W., and Arp, A. J. (2000) Life in extreme environments: Hydrothermal vents. *Proc. Natl. Acad. Sci. U. S. A.* **97**, 12961–12962
61. Tawfik, D. S., and van der Donk, W. A. (2016) Biocatalysis and biotransformation: Esoteric, niche enzymology. *Curr. Opin. Chem. Biol.* **31**, v–vii
62. Davidi, D., Shamshoum, M., Guo, Z., Bar-On, Y. M., Prywes, N., Oz, A., Jablonska, J., Flamholz, A., Wernick, D. G., Antonovsky, N., de Pins, B., Shachar, L., Hochhauser, D., Peleg, Y., Albeck, S., et al. (2020) Highly active rubiscos discovered by systematic interrogation of natural sequence diversity. *EMBO J.* **39**, e104081
63. Vickers, C. J., Fraga, D., and Patrick, W. M. (2021) Quantifying the taxonomic bias in enzymology. *Protein Sci.* **30**, 914–921
64. Lesley, S. A., Kuhn, P., Godzik, A., Deacon, A. M., Mathews, I., Kreusch, A., Spraggon, G., Klock, H. E., McMullan, D., Shin, T., Vincent, J., Robb, A., Brinen, L. S., Miller, M. D., McPhillips, T. M., et al. (2002) Structural genomics of the *Thermotoga maritima* proteome implemented in a high-throughput structure determination pipeline. *Proc. Natl. Acad. Sci. U. S. A.* **99**, 11664–11669
65. Liu, H., and Naismith, J. H. (2008) An efficient one-step site-directed deletion, insertion, single and multiple-site plasmid mutagenesis protocol. *BMC Biotechnol.* **8**, 91
66. Gasteiger, E., Hoogland, C., Gattiker, A., Duvaud, S., Wilkins, M. R., Appel, R. D., and Bairoch, A. (2005) Protein identification and analysis tools on the ExPASy server. In: Walker, J. M., ed. *The Proteomics Protocols Handbook*, Humana Press, Totowa, NJ: 571–607
67. Dou, C., Xia, D., Zhang, L., Chen, X., Flores, P., Datta, A., and Yuan, C. (2005) Development of a novel enzymatic cycling assay for total homocysteine. *Clin. Chem.* **51**, 1987–1989
68. McPhillips, T. M., McPhillips, S. E., Chiu, H. J., Cohen, A. E., Deacon, A. M., Ellis, P. J., Garman, E., Gonzalez, A., Sauter, N. K., Phizackerley, R. P., Soltis, S. M., and Kuhn, P. (2002) Blu-ice and the distributed control system: Software for data acquisition and instrument control at macromolecular crystallography beamlines. *J. Synchrotron Radiat.* **9**, 401–406
69. Kabsch, W. (2010) XDS. *Acta Crystallogr. D Biol. Crystallogr.* **66**, 125–132
70. Adams, P. D., Afonine, P. V., Bunkoczi, G., Chen, V. B., Echols, N., Headd, J. J., Hung, L. W., Jain, S., Kapral, G. J., Grosse Kunstleve, R. W., McCoy, A. J., Moriarty, N. W., Oeffner, R. D., Read, R. J., Richardson, D. C., et al. (2011) The Phenix software for automated determination of macromolecular structures. *Methods* **55**, 94–106
71. Emsley, P., and Cowtan, K. (2004) Coot: Model-building tools for molecular graphics. *Acta Crystallogr. D Biol. Crystallogr.* **60**, 2126–2132